Clinical and Translational Radiation Oncology 7 (2017) 71–78

Contents lists available at ScienceDirect

Clinical and Translational Radiation Oncology

journal homepage: www.elsevier.com/locate/ctro

Case Report

Increasing genomic instability during cancer therapy in a patient with Li-Fraumeni syndrome

Nadine Schuler [a], Jan Palm [a], Sabine Schmitz [b], Yvonne Lorat [a], Claudia E. Rübe [a,*]

[a] Department of Radiation Oncology, Saarland University, D-66421 Homburg/Saar, Germany
[b] Department of Safety and Radiation Protection, Forschungszentrum Jülich GmbH, D-52425 Jülich, Germany

ARTICLE INFO

Article history:
Received 21 June 2017
Revised 5 October 2017
Accepted 7 October 2017
Available online 2 November 2017

Keywords:
Li-Fraumeni syndrome
P53
Genomic instability
Craniospinal irradiation
Hematopoiesis

ABSTRACT

Background: Li-Fraumeni syndrome (LFS) is a cancer predisposition disorder characterized by germline mutations of the p53 tumor-suppressor gene. In response to DNA damage, p53 stimulates protective cellular processes including cell-cycle arrest and apoptosis to prevent aberrant cell proliferation. Current cancer therapies involve agents that damage DNA, which also affect non-cancerous hematopoietic stem/progenitor cells. Here, we report on a child with LFS who developed genomic instability during craniospinal irradiation for metastatic choroid plexus carcinoma (CPC).

Case presentation: This previously healthy 4-year-old boy presented with parieto-temporal brain tumor, diagnosed as CPC grade-3. Screening for cancer-predisposing syndrome revealed heterozygous p53 germline mutation, leading to LFS diagnosis. After tumour resection and systemic chemotherapy, entire craniospinal axis was irradiated due to leptomeningeal seeding, resulting in disease stabilization for nearly 12 months. Blood lymphocytes of LFS patient (p53-deficient) and age-matched tumor-children (p53-proficient) were collected before, during and after craniospinal irradiation and compared with asymptomatic carriers for identical p53 mutation, not exposed to DNA-damaging treatment. In p53-deficient lymphocytes of LFS patient radiation-induced DNA damage failed to induce cell-cycle arrest or apoptosis. Although DNA repair capacity was not impaired, p53-deficient blood lymphocytes of LFS patient showed significant accumulation of 53BP1-foci during and even several months after irradiation, reflecting persistent DNA damage. Electron microscopy revealed DNA abnormalities ranging from simple unrepaired lesions to chromosomal abnormalities. Metaphase spreads of p53-deficient lymphocytes explored by mFISH revealed high amounts of complex chromosomal aberrations after craniospinal irradiation.

Conclusions: Tumor suppressor p53 plays a central role in maintaining genomic stability by promoting cell-cycle checkpoints and apoptosis. Here, we demonstrate that a patient with LFS receiving craniospinal irradiation including large volumes of bone marrow developed progressive genomic instability of the hematopoietic system. During DNA-damaging radiotherapy, genome-stabilizing mechanisms in proliferating stem/progenitor cells are perturbed by p53 deficiency, increasing the risk of cancer initiation and progression.

Introduction

Li-Fraumeni syndrome (LFS) is a rare familial cancer predisposition syndrome with autosomal-dominant inheritance [1]. Over 250 germline mutations have been described throughout the TP53 tumor-suppressor gene that codes for the p53 protein [2]. As the guardian of the genome, p53 protects cells from many types of DNA damage by activation of cell cycle arrest, which allows the DNA damage machinery to repair genomic damage. In the setting of irreversible damage, p53 activation leads to apoptosis or senescence [3]. A broad range of tumors affect individuals with LFS from childhood through to adulthood, and are characterized by their early age of onset. Choroid plexus carcinomas (CPCs) are rare brain tumors that arise from the epithelium of choroid plexus of cerebral ventricles. Approximately 40% of CPCs occur in patients with LFS, which can influence management and confers a poorer prognosis

Abbreviations: CPC, choroid plexus carcinoma; DSBs, double-strands breaks; LFS, Li-Fraumeni syndrome; mFISH, multicolour fluorescence in-situ hybridization; NHEJ, non-homologous end-joining; SEM, scanning electron microscopy; TEM, transmission electron microscopy; γH2AX, phosporylated histone H2AX; 53BP1, 53 Binding Protein 1.

* Corresponding author at: Department of Radiation Oncology, Saarland University, Kirrbergerstrasse Building 6.5, 66421 Homburg/Saar, Germany.
E-mail address: claudia.ruebe@uks.eu (C.E. Rübe).

https://doi.org/10.1016/j.ctro.2017.10.004
2405-6308/

[4,5]. Total resection of CPC is associated with improved overall survival, but for patients with incompletely resected CPCs, chemo- and/or radiotherapy may be beneficial [6]. Double-strand breaks (DSBs), the most deleterious DNA lesions, are produced to great extent when cells are exposed to ionizing radiation and certain chemotherapeutics. The major mammalian pathway for DSB repair is non-homologous end joining (NHEJ), which occurs throughout the cell cycle [7]. NHEJ depends on the recognition of DSBs by Ku70-Ku80 heterodimer, which keeps broken DNA ends together until the breaks are finally rejoined [8–10]. Several proteins involved in DNA damage signaling produce discrete foci in response to ionizing radiation, and visualization of DNA-damage foci such as γH2AX or 53BP1 by fluorescence microscopy has been used to quantify radiation-induced DSBs [11,12].

Due to defects in cell cycle arrest and apoptosis DNA-damaging cancer therapy of patients with germline TP53 mutations may affect genome stability. Here, we report on a 4-year-old child with LFS who developed progressive genomic instability during fractionated irradiation of the craniospinal axis for metastatic CPC.

Material and methods

TP53 genotyping

Sequence analysis revealed the same heterozygous TP53 mutation (p53-mut; exon 8: c.916 > T, p.Arg306Stop) in this 4-year-old boy diagnosed with CPC and his 10-year-old sister and mother, neither of whom was diagnosed with active cancer.

Radiotherapy

Computer-tomography planning was performed to delineate target volume and critical structures. After three-dimensional conformal radiotherapy planning craniospinal axis was irradiated with 1.8 Gy daily (total dose 36 Gy) at the linear accelerator (Artiste™, Siemens, München, Germany; 6-MV photons; dose-rate 2 Gy/min).

Blood sampling

To analyse the DSB-repair kinetics, cell-cycle distribution and apoptosis, isolated lymphocytes were irradiated (*ex-vivo*) with 2 Gy. To evaluate foci accumulation during craniospinal irradiation (*in vivo*), blood samples were taken before treatment, 0.5 h after first fraction and 24 h after 1×, 5×, 10×, 15×, 20× fractions. To analyse long-term effects, blood lymphocytes were analysed 1, 2, 3, and 4 months after craniospinal irradiation.

Flow-cytometric analysis

Peripheral blood lymphocytes were stimulated by phytohemagglutinin (PHA, Chromosomen medium B, Biochrom, Berlin, Germany), irradiated *ex-vivo* with 2 Gy and allowed to recover in the presence of PHA. 24 h after *ex-vivo* irradiation, lymphocytes were fixed in paraformaldehyde and permeabilised in Triton-X100. After blocking nonspecific binding, cells were incubated with anti-Caspase3 antibody (R&D systems, Minneapolis, MN, USA) followed by anti-APC-Cy7 antibody (Santa Cruz Biotechnology, Heidelberg, Germany). To assess cell-cycle phase, cells were stained with propidium iodide (BD Biosciences, Heidelberg, Germany). For quantitative analysis, ≈10.000 cells were analysed using forward and side scatter parameters and gated into cell-cycle phases. For G0/G1 and S/G2 cells, staining intensities before and after irradiation were compared using the median of APC-Cy7 fluorescence signal. Data for each time point are presented as means from three different experiments.

Foci analysis

At defined time-points post-irradiation (*ex-vivo* or *in vivo*), isolated blood lymphocytes were spotted onto coverslips, fixed in methanol, and permeabilised in acetone. Samples were then incubated with anti-53BP1 (Bethyl, Montgomery, TX, USA) and/or γH2AX (Merck Chemicals, Darmstadt, Germany) antibodies followed by Alexa-Fluor-488 and/or Alexa-Fluor-568 conjugated antibodies (Invitrogen, Karlsruhe, Germany). Afterwards, samples were mounted in VECTAshield with 4′,6-diamidino-2-phenylindole (VectorLaboratories, Burlingame, CA, USA). DNA-damage foci were counted using an E600-epifluorescent microscope (Nikon, Düsseldorf, Germany) until at least 40 cells or 40 foci were scored for each data point.

TEM analysis

Blood lymphocytes were fixed, dehydrated in alcohol series, infiltrated with LR Gold resin™ (EMS, Hatfield, PA), embedded in fresh resin with benzil (EMS), and polymerised with ultraviolet light. Ultrathin sections were cut on Ultracut UCT Leica™ (Diatome, Biel, Switzerland), picked up with pioloform-coated nickel grids, and processed for immunogold-labelling. Sections were incubated with primary antibodies (anti-53BP1, Bethyl Laboratories; anti-pKu70 (pSer6), Abcam Inc., Cambridge, MA, USA) followed by antibodies conjugated with 6 or 10-nm gold particles (EMS). Subsequently, sections were rinsed and post-fixed with glutaraldehyde. All sections were stained with uranyl acetate and examined with TecnaiBiotwin™ transmission electron microscope (FEI Company, Eindhoven, Netherlands).

Scanning-electron microscopy (SEM) analysis

Metaphase chromosomes were prepared from cultured peripheral blood cells as described previously [13]. Cell suspensions were dropped onto slides, and chromosomes were fixed in glutaraldehyde and stained with chloro(2,2′:6′2″terpyridine)platinum(II)chloride-dehydrate (Sigma Aldrich). Subsequently, slides were washed and dehydrated in ethanol series. Chromosomes were chemically dried and evaporated with 3-nm carbon layers (BALTEC SCD030 sputter coater). Images were taken with an FEI/Philips XL30 FEG ESEM with Electron Backscatter Diffraction analysis at <5 kV accelerating voltage.

Multicolor fluorescence in-situ hybridization (mFISH) analysis

Metaphase spreads were hybridised with directly labelled 24XCyte mFISH specific probes (Multicolour FISH Probe Kit, MetaSystems, Altlussheim, Germany) [13]. Metaphase cells were searched with Zeiss Axioplan2 Imaging epifluorescent microscope (Zeiss, Oberkochen, Germany) and Metafer4/MSearch/AutoCapt imaging system (MetaSystems, Altlussheim, Germany). Fluorescent images were analysed with ISIS software (MetaSystems). Only spreads containing the full set of 46 chromosomes were scored.

Statistical analysis

Statistical comparisons were performed by Mann–Whitney test using OriginPro software. The criterion for statistical significance was $p \leq 0.05$.

Results

Case presentation

In March 2013, the third child of unrelated parents from Algeria presented with right parieto-temporal brain tumor diagnosed as

CPC grade-3 (Fig. 1A). Screening for cancer-predisposing syndromes revealed heterozygous TP53 mutation (exon 8: c.916 > T, p.Arg306Stop) for this 4-year-old boy, as well as for his 10-year-old sister and his mother, both without cancer diagnosis (healthy carriers, p53-mut). After surgical resection, LFS patient received systemic chemotherapy (etoposide, vincristine, cyclophosphamide) according to CPT-SIOP-2009 protocol (Fig. 1A). Due to tumour progression with neuroaxis dissemination, chemotherapy was changed to Irinotecan and Temozolomide. Subsequently, LFS patient received craniospinal irradiation (Fig. 1B), which resulted in disease stabilization. Under continued chemotherapy with Temozolomide and Topotecan intrathecal his health condition remained stable without neurological deficits. In June 2014, LFS patient suffered disease progression with multiple growing tumor lesions and brain stem involvement (Fig. 1A).

53BP1-foci as marker for radiation-induced DNA damage

To analyse DSB repair capacity, blood lymphocytes were irradiated *ex-vivo* with 2 Gy to determine induction at 0.5 h and to capture foci loss within 8 and 24 h after exposure (Fig. 2A). Compared to healthy individuals (p53-wt), p53-deficient lymphocytes from family members (p53-mut) revealed higher background levels and slightly higher foci levels at 8 and 24 h post-IR (Fig. 2B). Significantly, p53-deficient lymphocytes of LFS patient showed clearly higher induction values and considerably increased foci numbers at 8 h and 24 h post-irradiation (Fig. 2B). The kinetics for 53BP1-foci loss might be explained by higher amounts of pre-existing DNA damage, probably induced by previously administered chemotherapy. In addition, p53 may also directly impact the activity of various DNA repair systems, such as DSB repair by NHEJ [14]. Subsequently, we analysed persisting foci in blood lymphocytes during and after completion of radiotherapy. While p53-proficient lymphocytes (p53-wt) of an age-matched medulloblastoma patient revealed no foci accumulation during craniospinal irradiation (horizontal lines, Fig. 2C), foci levels of LFS patient increased from ≈0.5 to ≈1.5 foci/cell at completion of radiotherapy (Fig. 2C). After radiotherapy, blood lymphocytes of LFS patient revealed huge amounts of small 53BP1-foci, not co-localizing with γH2AX (Suppl. 1), potentially reflecting 53BP1 recruitment to damaged chromatin.

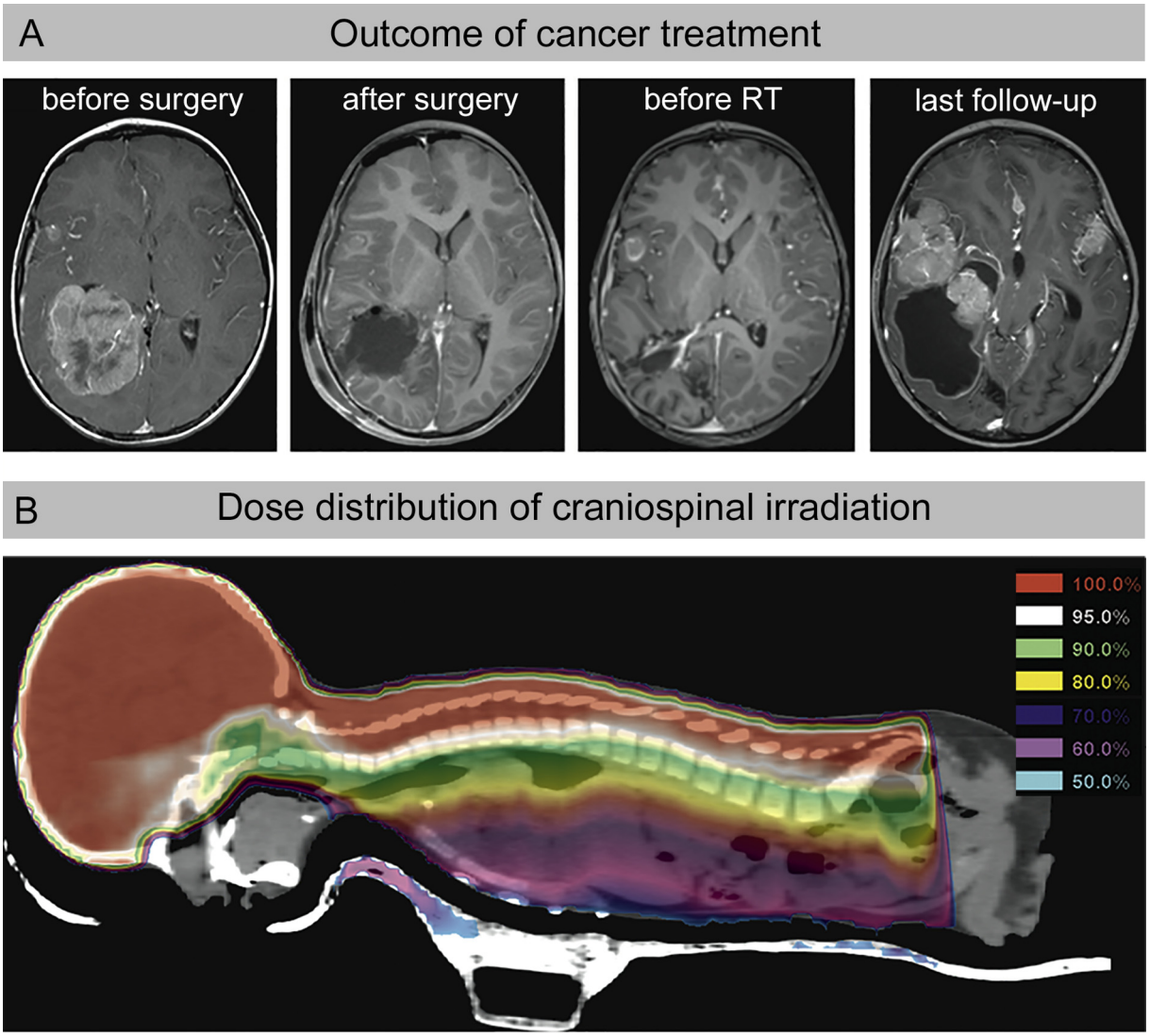

Fig. 1. Tumor therapy of the LFS patient. A: Evaluation of the treatment response by magnetic resonance tomography (MRT): T1-weighted images acquired in axial plane reveals the choroid plexus carcinoma (CPC) with enlargement of the ventricle before and after tumour resection and adjuvant radio-/chemotherapy. B: Craniospinal irradiation includes large volumes of active bone marrow. Colour-wash presentation illustrates the dose distribution. (For interpretation of the references to colour in this figure legend, the reader is referred to the web version of this article.)

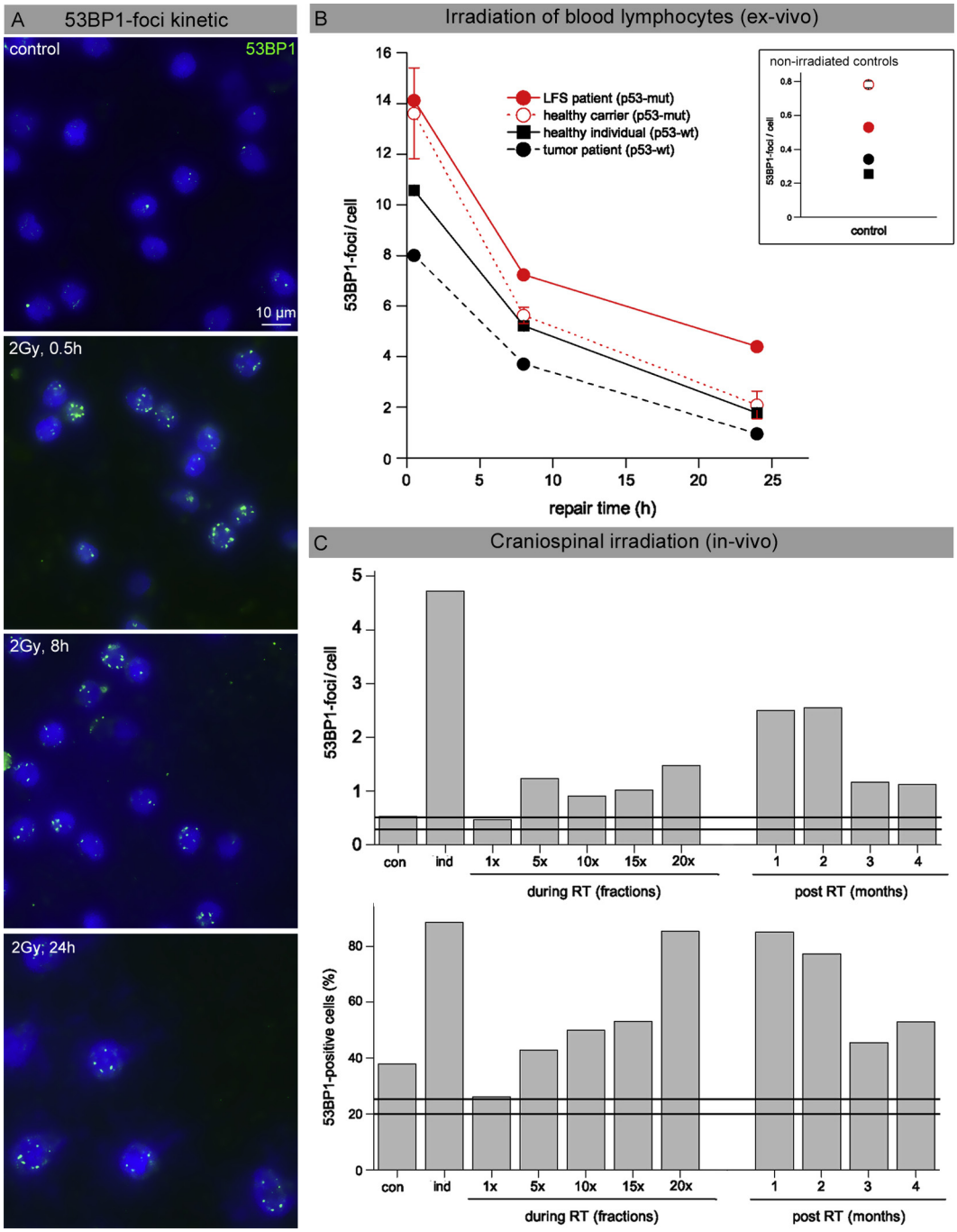

Fig. 2. 53BP1-foci as a marker for radiation-induced DNA damage. A: Immunohistochemical staining of 53BP1 in blood lymphocytes of a healthy individual analyzed 0.5, 8, and 24 h after *ex-vivo* irradiation with 2 Gy, compared to non-irradiated control. B: DNA repair capacity: 53BP1-foci were measured in blood lymphocytes from LFS patient (p53-mut), healthy TP53 carriers (p53-mut), and healthy individuals (p53-wt) and tumor-patient (p53-wt) at defined time-points after *ex-vivo* irradiation with 2 Gy. Inset shows 53BP1-foci levels in non-irradiated blood lymphocytes. C: Gradual accumulation of persisting 53BP1-foci during craniospinal irradiation (*in vivo*) of LFS patient (p53-mut), compared to the tumor-patient (p53-wt). 53BP1 foci were quantified 0.5 h (induction) and 24 h after the first fraction (1×), 24 h after 5×, 10×, 15× and 20× fractions (1.8 Gy), as well as 1, 2, 3 and 4 months after completion of RT. 53BP1-foci levels in the tumor-patient (p53-wt) did not increase during craniospinal irradiation (horizontal lines).

Radiation-induced cell cycle arrest and apoptosis

To analyze G1 arrest following radiation-induced DNA damage, PHA-stimulated p53-proficient blood lymphocytes from healthy individuals and p53-deficient lymphocytes from LFS patient were analyzed by flow cytometry 24 h after *ex-vivo* irradiation. In healthy individuals (p53-wt) most lymphocytes were in G0/G1 phase, with very low peripheral S/G2-phase cells and no appreciable damage-induced cell fragmentation, independent of *ex-vivo* blood irradiation (Fig. 3A). Monitoring of serial lymphocyte counts from LFS patient (p53-mut) revealed persistent severe lymphopenia due to constant radiochemotherapy application. Accordingly, analyzing cell-cycle distribution, we observed low percentages of mature G0/G1 cells with small subsets of S/G2 cells, but high amounts of cell fragments, represented by sub-G1 peaks of DNA histogram (Fig. 3A). Due to repetitive genotoxic insults by

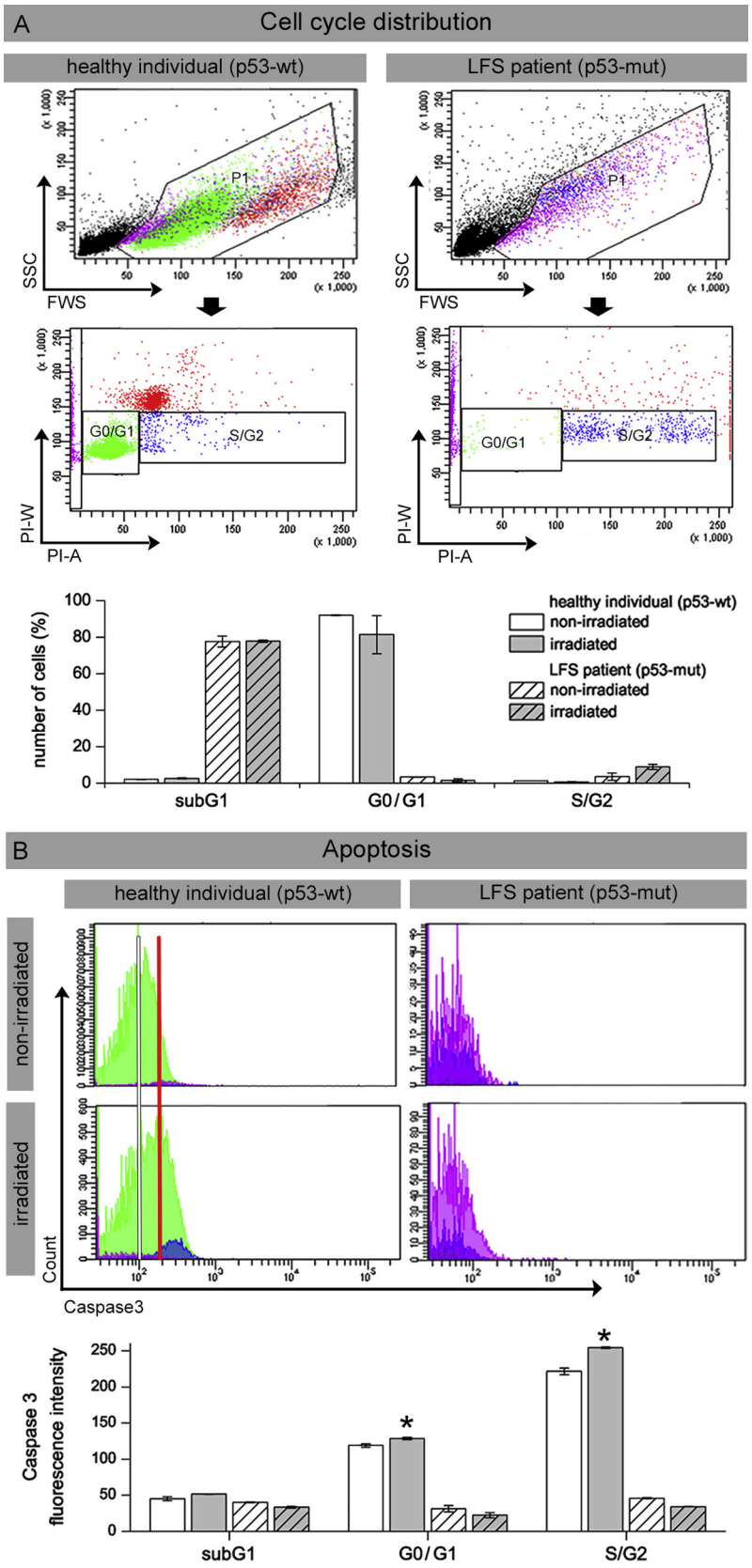

Fig. 3. Radiation-induced cell cycle arrest and apoptosis analysed by flow cytometry Blood lymphocytes from the LFS patient were analyzed before and after *ex-vivo* irradiation with 2 Gy, compared to healthy individuals. A: Cell cycle distribution determined with propidium iodide DNA staining: Analysis gates were set on forward versus side scatter to exclude debris and cell aggregates and to delineate subG1 (purple), G0/G1 (green) and S/G2 population (blue) (upper panel). B: Induction of Caspase3-dependent apoptosis: Median fluorescence intensity was measured in lymphocytes from LFS patient before and after *ex-vivo* irradiation with 2 Gy, compared to healthy individuals. In contrast to the LFS patient, healthy lymphocytes in G0/G1 and S/G2 phase show high Caspase3 intensity, particularly after irradiation (red line, left panel). Data from 3 different experiments are presented as mean ± standard equivalent. *Significantly different compared with non-irradiated control ($p \geq 0.05$). (For interpretation of the references to colour in this figure legend, the reader is referred to the web version of this article.)

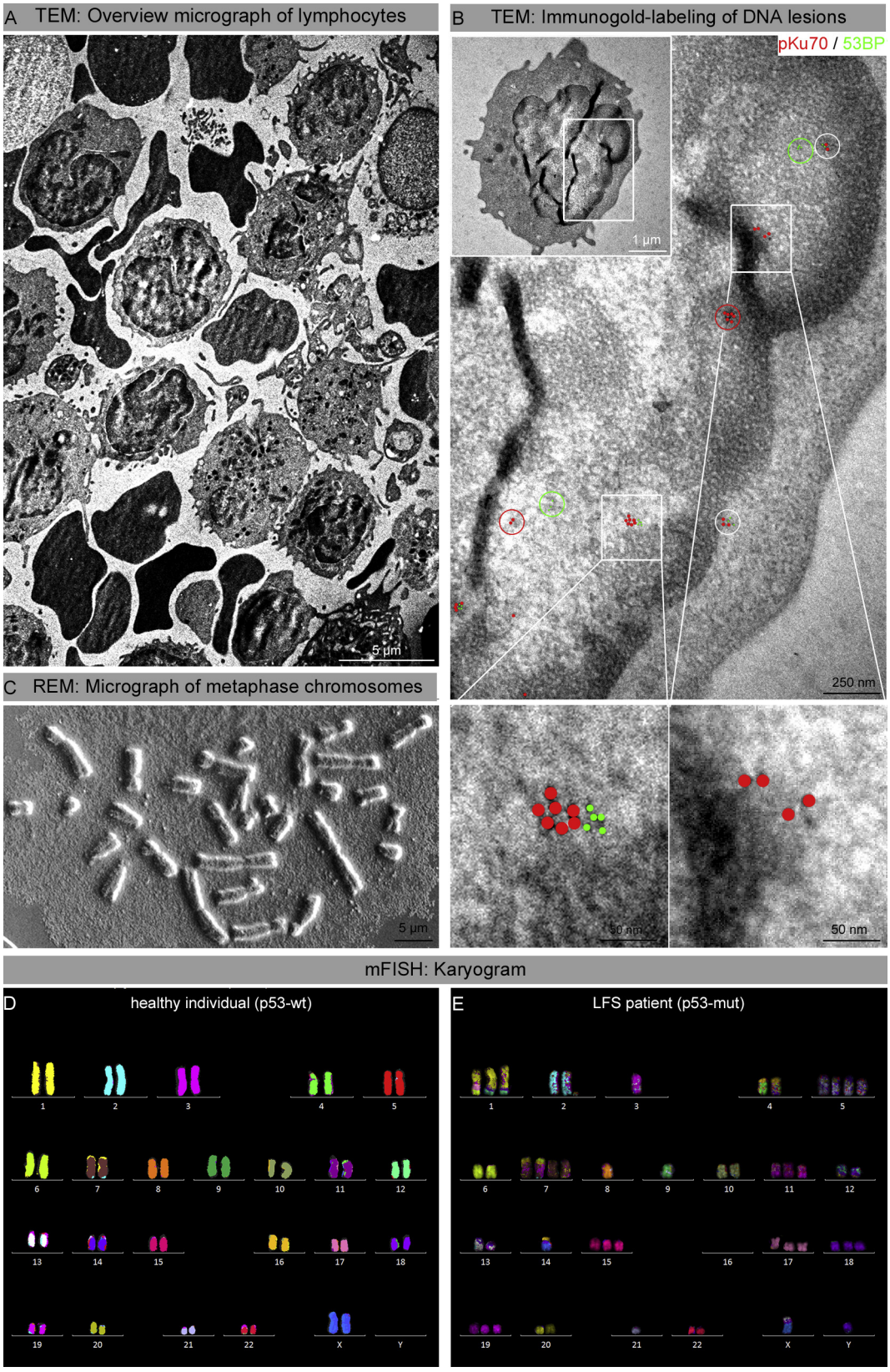

Fig. 4. Ultrastructural characterization of DNA lesions and chromosome analysis. Analyzed blood lymphocytes from the LFS patient were obtained 1 month after RT. A: TEM overview micrograph of peripheral blood lymphocytes. B: TEM micrographs of double-labeling of pKu70 (10-nm beads, red) and p53BP1 (6-nm beads, green) at different magnifications (boxed regions are shown at higher magnifications in the following images). Co-localization of pKu70 and 53BP1 in electron-dense regions, reflecting actively processed DSBs in heterochromatin. C: SEM micrograph of metaphase chromosomes of LFS patient reveals structural chromosome aberrations. D: mFISH Karyogram of the LFS patient (1 month after RT) shows multiple structural and numerical aberrations and can be described as follows: 49,XY,t(1;6;17),t(1;12),t(1;12),ace2,−3,t(4;16),t(4;16),+5,+5,del(6),del(6),+7,+7,t(6;7),t(6;7),−8,9,+11,t(12;1),t(12;1),add(13),t(13;X),−14,t(14;16),+15,del(16),del(16),+17,+18,+19−21. E: mFISH Karyogram of a healthy female individual. (For interpretation of the references to colour in this figure legend, the reader is referred to the web version of this article.)

Table 1
Quantification of structural and numerical chromosome aberrations.

	Σ analyzed metaphases	Fragments (ace)	Breaks	Deletions	Σ chromosome aberrations	Aberrant metaphases
Healthy individual (p53-wt)	257	12	3	2	6.6% (17)	3.9% (10)
Healthy carrier (p53-mut)	84	6	0	1	8.3% (7)	8.3% (7)
LFS patient (p53-mut)	39	10	1	3	35.9% (14)	28.2% (11)

radiochemotherapy, mature leukocytes may become fragile and perish during cytometric analysis. After *ex-vivo* irradiation we observed slightly higher values for S/G2 cells, suggesting that radiation-induced damage has no anti-proliferative impact, because of defective G1 arrest in p53-deficient cells. However, treatment-related lymphopenia may not only be the result of cytotoxic insults on mature leukocytes, but of the depletion of stem cell reserves. Immunocytochemical detection of Caspase-3 concurrent with DNA counterstaining enables the relation of apoptosis induction with cell-cycle phase (Fig. 3B). Flow cytometric measurement of blood lymphocytes from healthy individuals revealed an increase of Caspase-3 fluorescence intensity after irradiation (Fig. 3B, upper panel), detectable in all cell-cycle phases (Fig. 3B, lower panel). However, for LFS patient we observed extremely low Caspase-3 levels, independent from cell-cycle phase or sample irradiation (Fig. 3B). In p53-proficient blood lymphocytes from healthy individuals, we observed extremely low numbers of S/G2-phase cells, but an increase of Caspase-positive cells after radiation exposure. These findings indicate that blood lymphocytes with functional p53 pathways undergo G0/G1 arrest or apoptosis when treated with ionizing radiation. In p53-deficient lymphocytes of the LFS patient, by contrast, we observed no DNA damage-dependent cell cycle arrest and no efficient induction of apoptosis in response to radiation-induced DNA damage. Collectively, our findings support the notion that p53-mediated pathways help maintain genetic stability by preventing progression from G0/G1 into S phase and by the induction of apoptosis in response to radiation-induced DNA damage.

Ultrastructural analysis of DNA lesions by electron microscopy

To characterize the ultrastructure of persisting foci, gold-labeled repair proteins were visualized by transmission electron microscopy (TEM) (Fig. 4). TEM examination of p53-proficient lymphocytes of healthy individuals revealed only small 53BP1 clusters without any pKu70 binding, suggesting that all radiation-induced DSBs are repaired. Analyzing blood lymphocytes from LFS patient several months after radiotherapy, we observed clusters of pKu70 and 53BP1 beads occupying DNA sites in compact heterochromatin, reflecting persistently unrepaired DSBs (Fig. 4B). Scanning electron microscopy (SEM) analysis of metaphase preparations permits to visualize the gross morphology of chromosomes to detect gains and losses of chromosomal material. In metaphase preparations of the LFS patient, increased numbers of telocentric and acrocentric chromosomes and small chromosome fragments suggest that high amounts of genomic material got lost (Fig. 4C). However, these SEM analysis of metaphase preparations is insufficient to diagnose certain categories of abnormalities. SEM and TEM analysis of blood lymphocytes from healthy donors revealed no abnormalities.

Analysis of chromosome aberrations by mFISH

To achieve higher resolution of genomic changes, we performed chromosome-specific labelling by mFISH analysis [13]. In mFISH karyograms of LFS patient we observed multiple numerical aberrations. Moreover, heterogeneously stained regions with various overlapping fluorochromes (from each contributing chromosome) reflect structural exchanges of genomic material between different chromosomes, and were detectable in nearly all chromosomes of the LFS patient (Fig. 4D). For the LFS patient the frequency of chromosome aberrations after craniospinal irradiation was significantly increased; about 36% of metaphases revealed complex chromosome aberrations (Table 1). Due to fragility of blood lymphocytes after radiochemotherapy, only limited numbers of metaphase spreads could be analyzed for the LFS patient. Notably, the p53-deficient sister (p53-mut), who was not exposed to DNA-damaging cancer treatment, also revealed remarkable amounts of spontaneous chromosomal imbalances (Table 1). Translocation frequencies in peripheral blood lymphocytes are known to increase with age [15]. However, the frequency of chromosome aberrations of the healthy 30-years-old individual (p53-wt) was clearly lower compared to the 10-year-old p53-deficient sister (no cancer treatment) or the 4-year-old LFS patient (exposed to DNA-damaging cancer treatment). Collectively, these findings indicate that persistent dysregulation of the DNA damage response caused by germline p53 mutations cause genomic instability, particularly during cancer treatments inducing DNA damage.

Discussion

Tumor suppressor p53 eliminates or arrests the proliferation of damaged cells by induction of apoptosis and cellular senescence, and thus prevents DNA damage-induced genomic instability. In hematopoietic system accurate regulation of p53 activity is critical for balancing the fate of stem/precursor cells between self-renewal and differentiation in order to sustain the production of multilineage cells [16]. Here, we show in the clinical setting that LFS patient who underwent craniospinal irradiation revealed gradual accumulation of persistent DNA damage foci in peripheral blood lymphocytes. Considering the fairly short life-span of radiation-induced DNA damage, this foci accumulation during radiotherapy is probably not primarily the result of direct radiation exposure. In fact, our findings suggest that due to defects in radiation-induced cell cycle arrest and apoptosis p53-deficient hematopoietic stem/progenitor cells survived in face of radiation-induced DNA damage. Due to dysfunctional checkpoints, cell division with DNA lesions results in chromosomal mis-segregation during mitosis and thus, leads to pronounced cytogenetic abnormalities [17]. As result of genomic instability these aberrant hematopoietic stem/progenitor cells produce highly damaged progeny, which were to some extent mobilized into peripheral blood circulation.

The spectrum of TP53 mutations detected in the germline reflects those found in sporadic tumors. The majority of TP53 mutations occur within the DNA binding domain of the gene, primarily confined to highly conserved regions in the coding regions of exons 5–8 [18]. It is important to note that the germline mutation of the LFS patient is located in the coding region of exon 8, but doesn't belong to the most common mutations found in both sporadic tumors and in the germline. Accordingly, the functional significance of this specific germline mutation was unclear so far; particularly there was no information about increased radiosensitivity or associated genomic instability.

The sister of LFS patient, carrier for the same TP53 germline mutation, but without diagnosis or therapy of cancer, revealed slightly increased foci levels in non-irradiated blood lymphocytes

and increased numbers of chromosome aberrations, reflecting the inherent genome-destabilizing p53 pathway. In contrast, the age-matched child without p53 mutation, who was irradiated for medulloblastoma, did not show any accumulation of DNA damage foci nor genomic instability, in spite of aggressive DNA-damaging cancer therapy. These findings of differential DNA damage responses as a function of p53 status support the notion that coordinated progression through the cell cycle is crucial for maintenance of genome stability.

Conclusion

Dysfunction of p53 increases genomic instability in response to DNA-damaging cancer therapies, and thus enhances the risk of developing secondary malignancies.

Declarations

Ethics approval and consent to participate

The clinical protocol was approved by the local ethics committee, and parents of the patients provided written informed consent.

Consent for publication

The participants and/or their parents provided written informed consent for the publication of all relevant datasets.

Availability of data and materials section

The datasets used and/or analyzed during the current study are available from the corresponding author on reasonable request.

Competing interests

The authors declare that they have no competing interests.

Funding

This work was funded by the Federal Ministry of Education and Research (Grant-No. 02NUK035A).

Authors' contributions

NS: acquisition, analysis and interpretation of flow cytometry and foci data; statistical analysis.

JP: interdisciplinary patient management and acquisition of blood samples.

SS: acquisition, analysis and interpretation of mFISH data.

YL: acquisition, analysis and interpretation of SEM and TEM data.

CER: Conception and design, analysis and interpretation of data, acquisition of funding, manuscript preparation. All authors read and approved the final manuscript.

Acknowledgement

The authors would like to thank A. Isermann for editorial assistance in the preparation of the manuscript.

Appendix A. Supplementary data

Supplementary data associated with this article can be found, in the online version, at https://doi.org/10.1016/j.ctro.2017.10.004.

References

[1] Kamihara J, Rana HQ, Garber JE. Germline TP53 mutations and the changing landscape of Li-Fraumeni syndrome. Hum Mutat 2014;35:654–62.
[2] Leroy B, Fournier JL, Ishioka C, Monti P, Inga A, Fronza G, et al. The TP53 website: an integrative resource centre for the TP53 mutation database and TP53 mutant analysis. Nucleic Acids Res 2013;41:D962–9.
[3] Rufini A, Tucci P, Celardo I, Melino G. Senescence and aging: the critical roles of p53. Oncogene 2013;32:5129–43.
[4] Gozali AE, Britt B, Shane L, Gonzalez I, Gilles F, McComb JG, et al. Choroid plexus tumors; management, outcome, and association with the Li-Fraumeni syndrome: the Children's Hospital Los Angeles (CHLA) experience, 1991–2010. Pediatr Blood Cancer 2012;58:905–9.
[5] Tabori U, Shlien A, Baskin B, Levitt S, Ray P, Alon N, et al. TP53 alterations determine clinical subgroups and survival of patients with choroid plexus tumors. J Clin Oncol 2010;28:1995–2001.
[6] Sun MZ, Oh MC, Ivan ME, Kaur G, Safaee M, Kim JM, et al. Current management of choroid plexus carcinomas. Neurosurg Rev 2014;37:179–92 [discussion 92].
[7] Mahaney BL, Meek K, Lees-Miller SP. Repair of ionizing radiation-induced DNA double-strand breaks by non-homologous end-joining. Biochem J 2009;417:639–50.
[8] Williams GJ, Hammel M, Radhakrishnan SK, Ramsden D, Lees-Miller SP, Tainer JA. Structural insights into NHEJ: building up an integrated picture of the dynamic DSB repair super complex, one component and interaction at a time. DNA Repair (Amst) 2014;17:110–20.
[9] Lorat Y, Schanz S, Schuler N, Wennemuth G, Rube C, Rube CE. Beyond repair foci: DNA double-strand break repair in euchromatic and heterochromatic compartments analyzed by transmission electron microscopy. PLoS One 2012;7:e38165.
[10] Rube CE, Lorat Y, Schuler N, Schanz S, Wennemuth G, Rube C. DNA repair in the context of chromatin: new molecular insights by the nanoscale detection of DNA repair complexes using transmission electron microscopy. DNA Repair (Amst) 2011;10:427–37.
[11] Lukas J, Lukas C, Bartek J. More than just a focus: the chromatin response to DNA damage and its role in genome integrity maintenance. Nat Cell Biol 2011;13:1161–9.
[12] Rube CE, Dong X, Kuhne M, Fricke A, Kaestner L, Lipp P, et al. DNA double-strand break rejoining in complex normal tissues. Int J Radiat Oncol Biol Phys 2008;72:1180–7.
[13] Schmitz S, Pinkawa M, Eble MJ, Kriehuber R. Persisting ring chromosomes detected by mFISH in lymphocytes of a cancer patient-a case report. Mutat Res 2013;756:158–64.
[14] Williams AB, Schumacher B. DNA damage responses and stress resistance: Concepts from bacterial SOS to metazoan immunity. Mech Ageing Dev 2017;165:27–32.
[15] Whitehouse CA, Edwards AA, Tawn EJ, Stephan G, Oestreicher U, Moquet JE, et al. Translocation yields in peripheral blood lymphocytes from control populations. Int J Radiat Biol 2005;81:139–45.
[16] Nii T, Marumoto T, Tani K. Roles of p53 in various biological aspects of hematopoietic stem cells. J Biomed Biotechnol 2012;2012:903435.
[17] Santaguida S, Amon A. Short- and long-term effects of chromosome mis-segregation and aneuploidy. Nat Rev Mol Cell Biol 2015;16:473–85.
[18] Malkin D. Li-Fraumeni syndrome. Genes Cancer 2011;2:475–84.